1-1-2017

Fracture Conductivity Modelling in Experimental Shale Rock Interactions with Aqueous CO_2

Abiola Olabode
Louisiana State University

Mileva Radonjic
Louisiana State University

Recommended Citation

Olabode, A., & Radonjic, M. (2017). Fracture Conductivity Modelling in Experimental Shale Rock Interactions with Aqueous CO_2. *Energy Procedia, 114*, 4494-4507. https://doi.org/10.1016/j.egypro.2017.03.1610

Available online at www.sciencedirect.com

ScienceDirect

Energy Procedia 114 (2017) 4494 – 4507

Energy Procedia

13th International Conference on Greenhouse Gas Control Technologies, GHGT-13, 14-18 November 2016, Lausanne, Switzerland

Fracture Conductivity Modelling in Experimental Shale Rock Interactions with Aqueous CO_2

Abiola Olabode[a]*, Mileva Radonjic[a]

[a]*Louisiana State University, 2131/2116 Patrick F.Taylor Hall, Baton Rouge 70803, USA*

Abstract

In large scale subsurface injection of carbondioxide (CO_2) as obtainable in carbon sequestration programs and in environmentally friendly hydraulic fracturing processes (using supercritical CO_2), long term rock-fluid interaction can affect reservoir and seal rocks properties which are essential in monitoring the progress of these operations. The mineralogical components of sedimentary rocks are geochemically active particularly under enormous earth stresses, which generate high pressure and temperature conditions in the subsurface. While geomechanical properties such as rock stiffness, Poisson's ratio and fracture geometry largely govern fluid flow characteristics in deep micro-fractured formations. Simulation results suggested that influx-induced mineral dissolution/precipitation reactions within clay-based sedimentary rocks can continuously close micro-fracture networks, though injection pressure and effective-stress transformation first rapidly expand the fractures. This experimental modelling research investigated the impact of in-situ geochemical precipitation on conductivity of fractures under geomechanical stress conditions. Bulk rock geomechanical hardness was determined using Vickers' micro-indentation. Differential pressure drop data across fractured composite core were also measured with respect to time over a five day period. This was used in estimating the conductivity of the artificially fractured cores with 25µm-bore microtubings embedded. Three experimental runs per sample types were carried out in order to check the repeatability of observed changes. The results showed that most significant diagenetic changes in shale rocks after flooding with CO_2-brine, reflect in the effluent fluid with predominantly calcium based minerals dissolving and precipitating under experimental conditions. Micro-indentation results suggested slight reduction in the hardness of the shale rocks and this reduction appears dependent on diagenetic quartz content. Estimated fracture conductivity indicated that reactive transport of dissolved minerals can occlude micro-fracture flow paths, thereby improving caprock seal integrity with respect to leakage risk under CO_2 sequestration conditions.

Peer-review under responsibility of the organizing committee of GHGT-13.

Keywords: diagenesis, fracture conductivity, micro-indentation, seal integrity, nanopores

Peer-review under responsibility of the organizing committee of GHGT-13.

doi:10.1016/j.egypro.2017.03.1610

1. Introduction

In naturally fractured geologic formations, conductivity of fractures are important in fluid extraction and injection. The role of mineralization in the loss of fracture conductivity due to aqueous precipitation of insoluble substances has been discussed by several researchers. It is generally thought that aside geomechanical properties of sedimentary rocks, the geochemical properties of rocks and reservoir fluids can favorably or unfavorably lead to the constriction of fractures in the subsurface given the right temperature, pressure and chemical composition [1]. This type of constrict is desired in CO_2 sequestration and containment. Different formation evaluation scales can be considered when describing tight shaly rocks (caprock): from the pore or grain scale in petrophysics and geochemistry, to regional scale in geology and geomechanics. For clayey caprocks, the amount and type of clay is critical in characterizing its petrophysics unlike tight carbonate formation where dolomitisation is the key feature [2]. When injecting CO_2, mechanical constraints are generated in both the storage and caprock formations, and the bottom of the caprock can be affected by geochemical reactions. Several studies have shown that in large scale carbon sequestration, the CO_2 migrates a few meters during one thousand years, and that the porosity mostly decreases by precipitation, and increases very locally at the base of the caprock by dissolution [3, 4, 5]. Naturally occurring fractures in shaly caprocks under CO_2 sequestration and subsurface fluid extraction make significant contribution to flow and any natural or artificial geologic process that can impact them should be adequately researched [6 – 10].

Diagenesis is the process of physical and chemical changes in sediment, after deposition that converts it to consolidated rock. Classical diagenesis is considered to be a slow process occurring over centuries, but in fact, the reactions occur fairly rapidly, requiring fractions of years at reservoir conditions. Common minerals, dissolved in or precipitated from an aqueous phase can be grouped into those that are relatively reactive or inert in that their dissolution or precipitation rates are fast or slow, respectively, relative to the flow rate of the aqueous phase. Multiple investigators have outlined the consequences of variations in reaction rates relative to flow rate of the fluid in which the minerals are reacting. These minerals can be further grouped according to simple and complex stoichiometry [11]. Those minerals with complex stoichiometry are much less likely to reach the solubility equilibrium than those with simple stoichiometry. Since calcite is a reactive mineral and has simple stoichiometry, it is considered as an example of water-rock reaction problem whenever it is present in substantial amounts [11, 1]. Physical, chemical, and organic processes begin acting on carbonate sediments after their deposition, leaving an influence on the mineral composition and structure. Diagenesis typically changes porosity, permeability and capillary pressure characteristics [7, 9, 12].

Experimental studies of wettability, contact angle and interfacial tension on shale using CO_2-rich fluid have not been widely reported but there are recent works along this line [13]. Porosity, permeability, fractures and other petrophysical properties of the seal rock are of importance in seal integrity analysis and can be experimentally determined [14]. Organic-rich shale is considered to have limited potential as membrane seals in CO2 containment [15, 16]. Shale rocks are predominantly composed of clay. They might also have other silica and carbonate based minerals that contribute to their geomechanical strength [17,18]. The geochemical reactivity of caprock formations should be evaluated gradually, essentially in two steps: classical batch experiments on crushed or small pieces of rock samples to evaluate reaction paths and possibly the reaction kinetics, and flow tests on plugs to evaluate, among other important quantities, the porosity variations [19]. Experiments conducted with shale and supercritical co2 containing traces of O_2 and other impurities show oxidative dissolution of pyrite and precipitation of iron oxide.

In long-term transport of CO_2, penetration depth of the aqueous fluid front in a saturated caprock layer is suggested to be dependent on the square root law for both pressuring time and pressure magnitude [5]. The presence of natural micro-fractures in these caprocks can accelerate transport rate in the subsurface, although any large scale leakage through natural subsurface storage traps seems to be limited to escape classical routes i.e., fractures and faults, rather than, being caused by chemical modifications of porosity [20]. Studies on natural CO_2 reservoirs offer limited data for CO_2/caprock interactions on field scale because the focus in most cases are on the reservoir rock properties and critical trace elements immobilization by acidic perturbation [21]. Dormant and filled fractures may be reactivated as a result of coupled chemical alteration, pressure buildup and thermal stresses. The results presented in this paper addressed the concerns that are associated with micro-fracture flow characteristics in caprocks under laboratory settings that attempts to replicate sedimentary reservoir conditions involving carbon sequestration.

2. Materials and Methods

The procedure used in characterization of the four different crushed shale rocks prior/post exposure to reactive CO2-brine fluid is described and it is followed by mineralogical analysis of the rock and geochemical analysis of the effluent fluid collected during the experiment. The experiments were carried out 3 times per sample type.

2.1. Experimental Setup

The experimental set-up consisted of a core flooding unit (CFS-200), an automated Oven, a heating tape, a stainless steel pressure cell, a syringe pump (and a piston pump for backup), a back pressure regulator (BPR), accumulators (glass beaker), multiple transducers, three pressure gauges, PEEK and stainless steel tubings, National Instruments device with differential pressure transducers for per second data acquisition, two ceramic filter to prevent fines carry over (larger than 50 μm) and a computer system. Schematics of the CO_2-brine flooding of shale caprock and composite fractured core used are shown in Figures 1 and 2 respectively.

Crushed samples of shale rocks from four different formations in the US. Samples A, B, C and D refer to Mancos, Marcellus, Pottsville and Wilcox shale respectively. They were flooded with CO_2-brine at gradually increased pressure in steps of 100 psi/hour up to a maximum of 1000psi. This gradual pressure increase was to prevent localized fluidization of the samples particularly during the first 10 hours of the start of the experiment.

The crushed samples are 1mm to 2mm in diameter. The crushing were done at the Engineering and Mining Experiment Station at Rapid City in South Dakota. Each experimental run included an average of 350g of shale samples and was subjected to a flow rate of 0.5cm^3/min at a regulated back pressure of 1000psi and50°C temperature throughout the three months of the experiment. The CO_2-brine fluid used during the experiment was prepared by bubbling CO_2 into a brine solution (0.35mol/liter NaCl) at 60 psi for 2hrs in a stainless steel storage tank. This yielded CO_2-brine pH of 3.7 on the average. Samples of shale rock were analysed over a five day period.

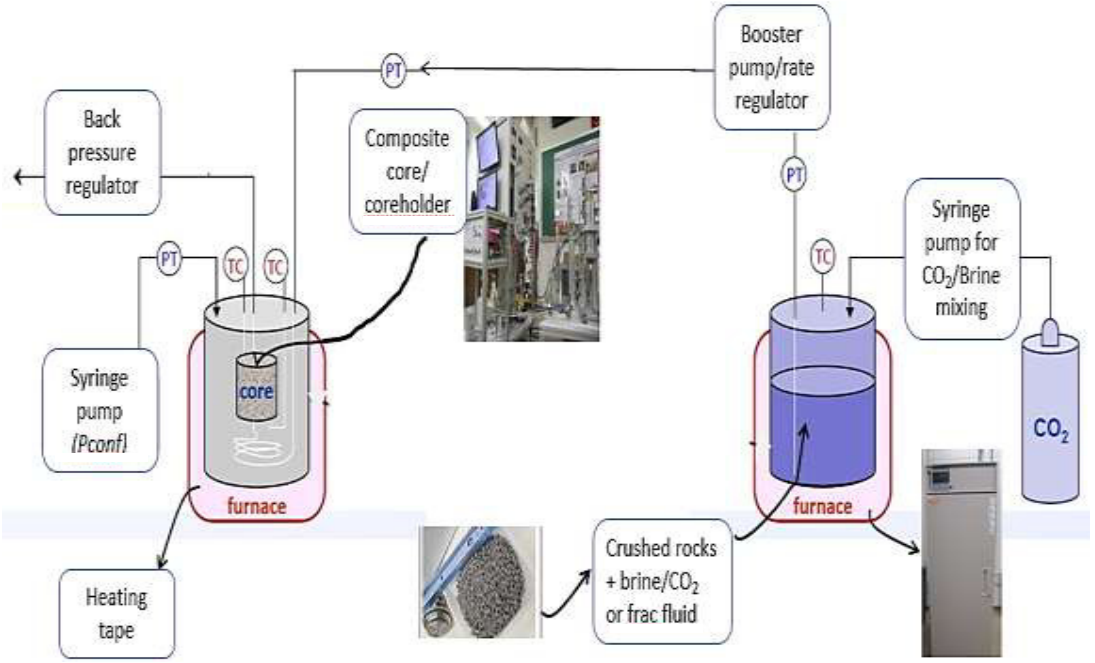

Fig. 1. Schematics of the process flow diagram of the experimental setup showing critical devices and equipment for CO_2-brine flooding and composite core conductivity. The experiments were conducted at 50 degree Celsius and 1000 psi injection pressure in noncorrosive environment. The experiments were carried out 3 times per sample type. This yielded multiple data points for statistical analysis and results verification.

It should be mentioned that the crushing of the shale rock samples was done in order to speed up rock fluid-interaction under laboratory setting. This is usually referred to as the GRI method. The phenomena observed are expected to represent short-term geologic event which may be in decade's time frame.

The liquid effluent was analyzed first for acidity using pH meter and later for cationic content using inductively coupled plasma – optical emission spectroscopy (ICP-OES). The results obtained were used to determine the extent of the impact of reactive CO_2-brine on the shale caprock integrity.

The packed-bed was mounted vertically in the oven for temperature control with aqueous CO_2 flowing from the top to the bottom of the experimental fixture. This is to prevent particulate fluidization. Levitation of colloidal particles that may be present were reduced significantly with the choice of flow direction.

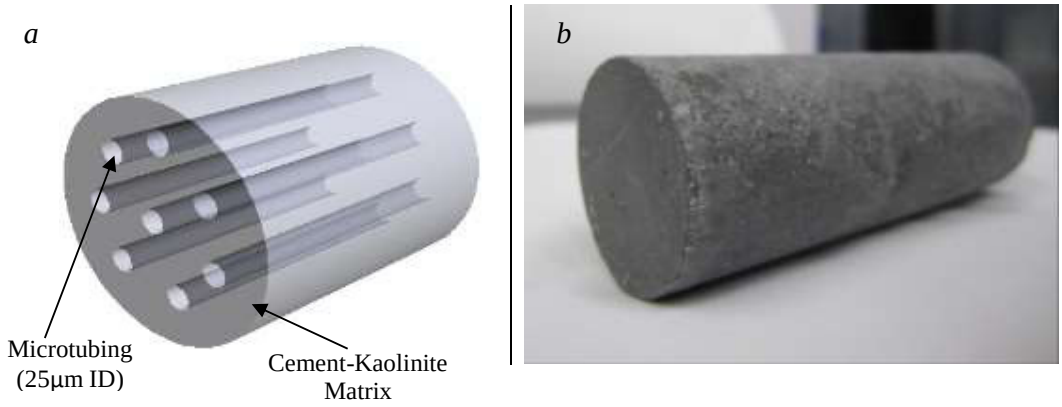

Fig. 2. (a) Visual design of composite core made of kaolinite, cement and microtubings (magnified) using SolidWorks©. (b) Visual sample design of composite core made of kaolinite, cement and polymer PEEK microtubings (25µm internal diameter) which are not evenly distributed as envisage through SolidWorks©.

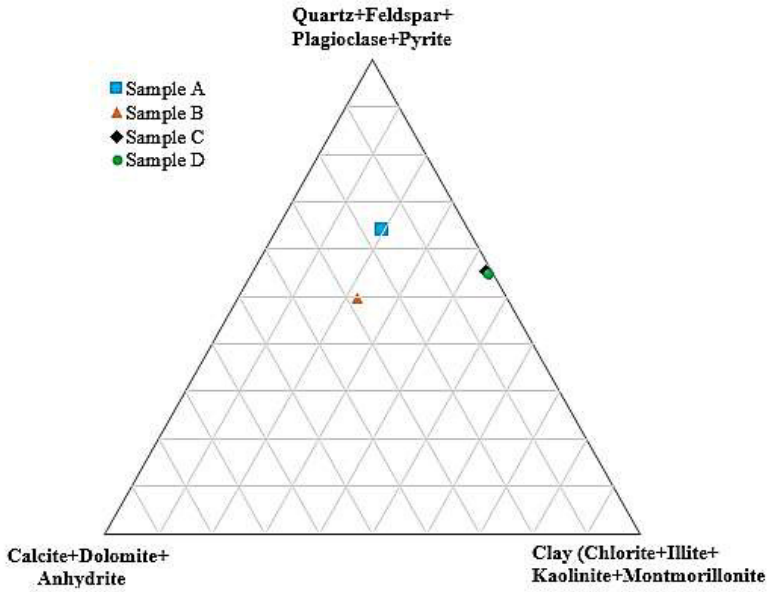

Fig. 3. Initial mineralogical composition of four shale rock samples (from XRD Analysis) used in rock-fluid interaction experiment. The ternary diagram shows carbonates, quartz, feldspar, pyrite and clay as main components of the shale rocks used for the experiment.

The ternary diagram in figure 3 shows the compositional distribution of the major minerals in the shale rock samples as determined from XRD analysis. Qualitative details of the percentage composition of each mineral can be deduced from the ternary diagram; the samples consist, on a broad scale, quartz, feldspar, pyrite, calcite, dolomite, anhydrite, chlorite, illite, kaolinite and montmorillonite as expected of sedimentary rocks. The relative abundance of these components in each shale rock type showed the preponderance of quartz, carbonates and clay in general terms.

2.2 Fluid Preparation and Rock Sampling

Carbon dioxide saturated brine solution was used for all experiments as the working reactive fluid. Brine was prepared with distilled/de-ionized water to ensure that unknown species were not present in the solution. The brine composition was designed to simulate typical shale formation brine as observed in hydraulic stimulation flowback water. This laboratory brine does not contained Mg^{2+} and Ca^{2+} salts in any amounts. The composition was then simplified to include only NaCl which contains trace amount of KCl (<0.005%). The brine solution contained ~ 22.6g salt solids to formulate total dissolved solution of 20,000ppm at the least. After mixing water and salts, the brine was filtered using filter paper to eliminate undissolved solid particles that can plug the flow lines in the experimental set-up. A filter was also installed upstream of injection to reduce the risk of plugging the flow lines by crystallizing salts. An accumulator (volume ~25 liters) was used to hold the brine solution as gaseous CO_2 was bubbled through at 60 psi for approximately 120 mins resulting in average pH value of 3.7 over the course of the experiment. This method was selected because of the ease of preparation. A digital pH meter was used to record pH measurements thrice every day and calibration was done with standard buffer solutions (pH= 4, 7, 10) each week.

Approximately 10g of each experimental rock samples were analyzed after the rock-fluid interaction process. This amount was sufficient for XRD analysis (Bulk and Clay) and TOC. Separate fragments of the shale rocks were selected from the center of the packed bed for micro-indentation and electron micro-probe analyses (EMPA). The results from XRD analysis and EMPA are discussed in another related conference article.

3. Results

The mineralogical composition of shale caprock plays a significant role in its ability to perform effectively as a regional seal. Different mineral compositions ranging from quartz, calcite, anorthites, feldspar to, chlorite, illite, kaolinite and montmorillonite have been reported for shale. Mineral dissolution, re-precipitation and redistribution may affect transport properties in microfractured shale and consequently their sealing capacity under carbon sequestration conditions. ICP-OES and micro-indentation techniques were used to probe fluid and rock geochemical activities before and after the experiment. Differential pressure drop across micro-fractured core was used in the estimation of fracture conductivity loss with respect to time. The results of the observed diagenetic responses as an outcome of rock-fluid interaction are discussed beginning with fluid and rock analysis and ending with flow characterization. Artificially fractured rocks were designed to mimic natural micro-fractures in shale.

3.1 ICP-OES Analysis of Effluent Fluid

3.1.1 Major Elements

Elemental Calcium concentration along with other alkaline earth metals in the effluent collected at the outlet of the artificially fractured cores are presented in figure 4. The ratios of Ca_n/Ca_o are presented as data points on the chart. Can represent the concentration of Calcium in part per million (ppm) for each day (n= time in days). Cao is the original elemental concentration in the influent CO_2 saturated brine. This dimensionless entity represents the fractional increase or decrease in the elemental composition of Calcium and other major alkaline earth metals discussed in this section (Magnesium (Mg), Potassium (K), Aluminum (Al), Iron (Fe) and Silicon (S)). The error bars are standard deviation values based on 3 measurements of elemental composition.

The concentration profile for Calcium (figure 4a) shows that Sample B had the highest fraction in solution which rapidly decreased over the five day period of continuously flooding the samples with CO_2 saturated brine. The initial pH of the influent fluid is approximately 3.7. Samples A, B and D exhibited similarly trend of a gradual exponential decline over the five day period. Sample C reflected a gradual increase that appears to continue over the experimental period. While the elemental concentration of Calcium in samples A, B and D peaks on the first day of the experiment, that of sample C continued to increase over the five day period but it also expected to peak and gradually decline with similar trend to samples A, B and D. This resilient behavior of sample C might suggest a slower dissolution reaction of it calcium based minerals constituent compared to samples A, B and D. The bulk rock XRD analysis indicated calcite and dolomite as the main calcium bearing minerals in samples A, B and D while anhydrites are the main calcium bearing minerals in sample C. Overall, samples A, B and D had significantly higher fraction of Ca within the first two days of the experiment compared to sample C indicating greater dissolution of calcium based minerals.

Figure 4b presents the five day elemental concentration trend in the effluent for Magnesium. The profile for the four samples are similar to that of calcium. It can be observed that the fractional composition of magnesium in the effluent are about half of elemental calcium presented in figure 4a. Samples A, C and D appear to be plateauing out after the five day experimental period, while sample B is rapidly approaching zero concentration during the same period. The similarity of concentration profile suggests that plausible geochemical dissolution reactions are occurring along with magnesium based minerals in the shale rocks. These type of reactions are mostly associated with calcite, dolomite and illitic (illite containing) clay minerals.

Elemental Potassium in solution exhibited a trend that showed a reduction in the free potassium available in the influent fluid for samples B and D before stabilizing after the five days experimental period (figure 4c). The profile for samples B and D indicated a marked reduction in potassium concentration beginning from the start of the experiment. This suggests that trace amount of K in the brine were absorbed. This indicated a consumption of the potassium element in the injected fluid via reactive rock-fluid interaction for the two samples. Samples A and C exhibited the general trend of initial increase in elemental (potassium) concentration in the effluent fluid followed by a decreasing profile as the experiment progresses.

Figure 4d shows the concentration of Al in the effluent solution for all the four samples used in the five day experiment at moderate temperature and pressure conditions. The concentration for samples B and D followed the trend observed in potassium concentration profile indicating a consumption of the element during possible reactive rock-fluid interaction. It is safe to assume that Aluminum did not participate significantly in these reactions given it low concentration in the effluent, though dissolved aluminum bearing minerals in solution could have precipitated out of the solution in form of clay, therefore the low concentration. Samples A and C showed little to no change in Al concentration indicating passive interaction of aluminum bearing minerals in these samples with CO_2-brine influent fluid. Overall, the concentrations of Al remained constant for samples A and C while those for samples B and D were initially mildly reduced but later held constant during the last three days of the experiment.

Elemental concentration of Iron is quite significant in sample D as shown in figure 4e. The profile showed that sample D had a much higher fraction of Fe in solution compared to the other three samples. This Fe concentration rapidly reduced over time during the experiment. The chart presents a confirmation that the pyrite (FeS_2) content in sample D reactively interacted more with the influent fluid leading to high concentrations of Iron (Fe) and Sulphur (S) in the effluent. Other samples (samples A, B and C) have iron concentration in trace amounts.

Elemental silicon concentration in the effluent analyzed showed that they are present in solution in significant quantity compared to the initial CO_2-brine fluid that was injected. Figure 4f documents these concentrations for all the shale samples. The fractional profile of silicon indicated dissolution of silicon bearing minerals. It is possible that early precipitation in form of diagenetic quartz occurred as the concentration of Si remained fairly constant. The presence of diagenetic quartz in the precipitates recovered, indicated that most of the silicon in solution had crystallized out of the solution to form a variant of opal mineral that is amorphous in shape.

These major elemental concentrations discussed showed that I the possible case of absorption, dissolution and exchange of cations in aqueous fluid under carbon sequestration conditions, alkaline earth metal based minerals would constituent the contents of diagenetic precipitates that will be formed. Calcium in particular will dominate dissolution-precipitation pathways when presence in significant amount. This was the trend observed when XRD analysis were carried out on the precipitates recovered from the effluent during the 5-day experiments.

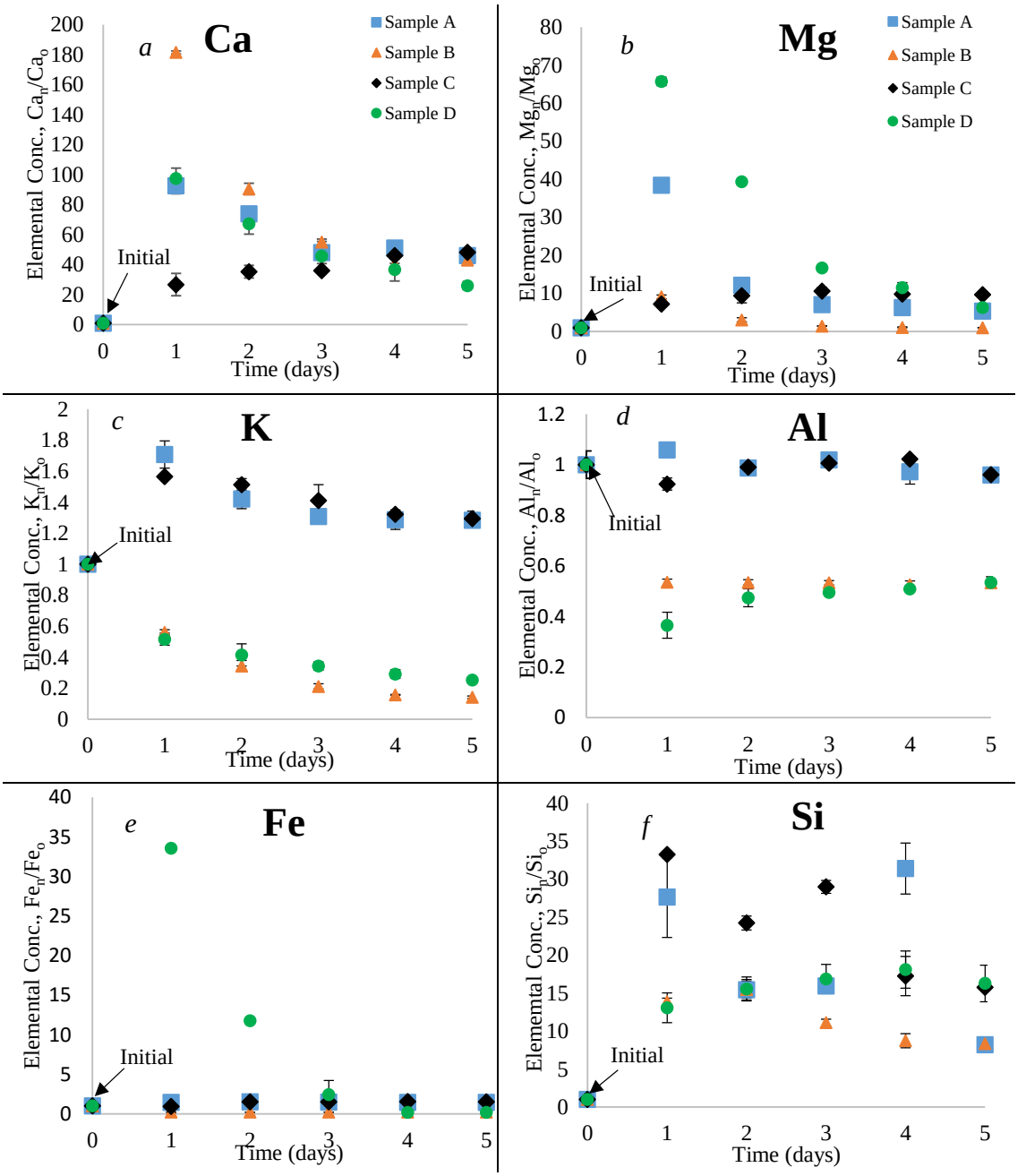

Fig. 4. Dimensionless cationic concentration of main elements in the effluent fluids showing the fraction of (a) Calcium (Ca) (b) Magnesium (Mg) (c) Potassium (K) (d) Aluminum (Al) (e) Iron (Fe) and (f) Silicon (Si) that were leached out from the shale rock samples. Concentrations vary significantly in the fluid samples analyzed. The effluent were diluted during the actual ICP-OES procedure and necessary corrections were made to capture the dilution. This was necessary as the extremely high concentration of dissolved NaCl tend to affect readings of other elemental components and the thermal bulb of the equipment could also be compromised at high temperature and salinity. The repeat measurements (as reflected in the error bars/standard deviation reported) helped ensure the accuracy of the reported geochemical data.

3.1.2 Minor Elements

Trace concentration of certain elements in the effluent solution is discussed. These include Manganese (Mn), Sulphur (S), Zinc (Zn), Selenium (Se), Phosphorus (P) and Nickel (Ni), Arsenic (As) and Boron (B). Dimensionless cationic concentration of the trace elements that were leached out from the shale rock samples are also presented. They are described as occurring in trace or minor amounts because any mineral associated with these element are either not picked by XRD analysis or occurs in very minute fraction in the bulk rock e.g pyrite. Previous researchers have attempted to model the mechanism behind the release of these trace metals and their evolution in carbonates reservoirs that are capped by shale rocks [7, 11].

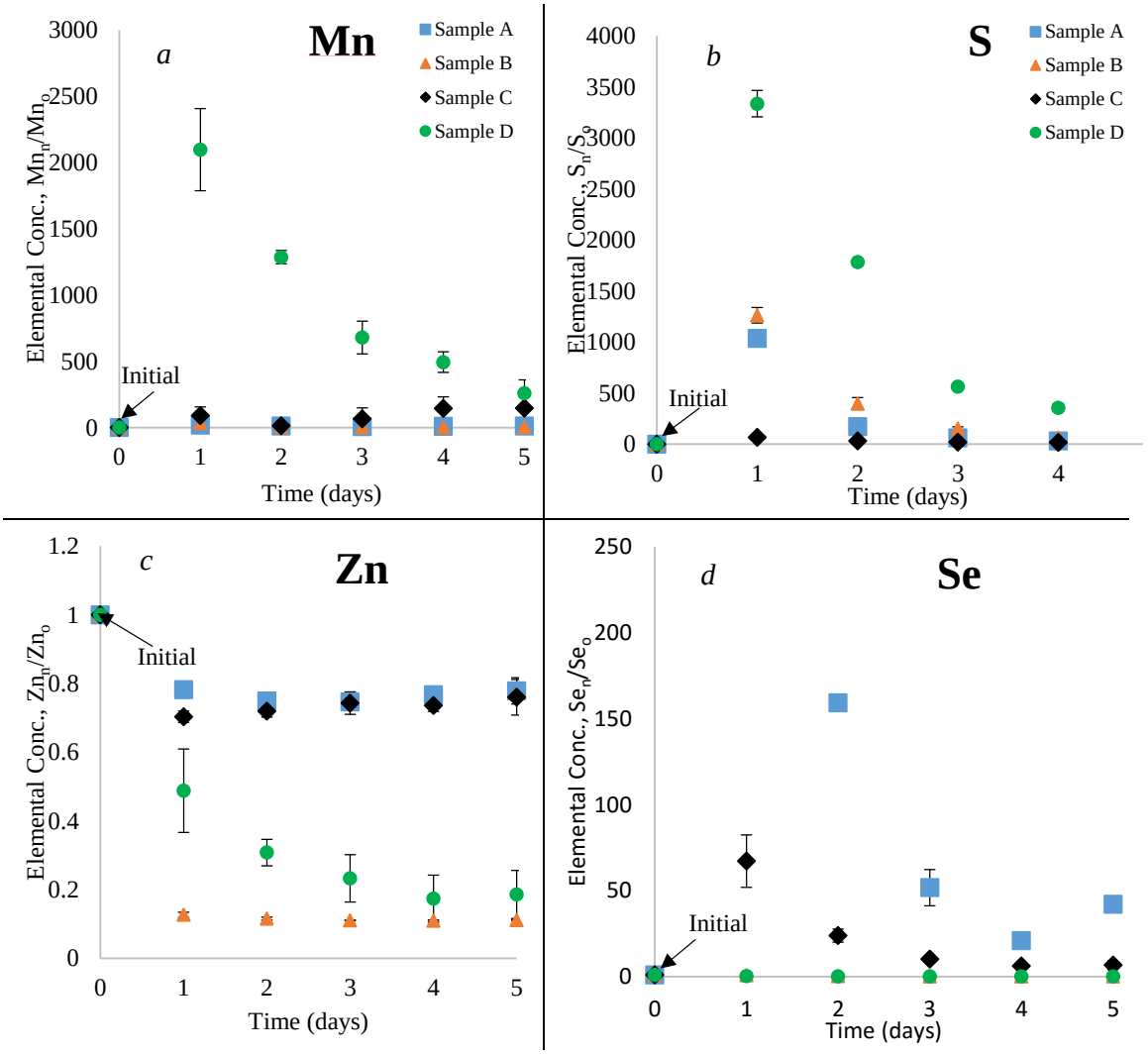

Fig. 5. Dimensionless cationic concentration of trace elements in the effluent fluids showing the fraction of (a) Manganese (Mn) (b) Sulphur (S) (c) Zinc (Zn) (d) Selenium (Se) that were leached out from the shale rock samples. Concentrations vary significantly for this elements.

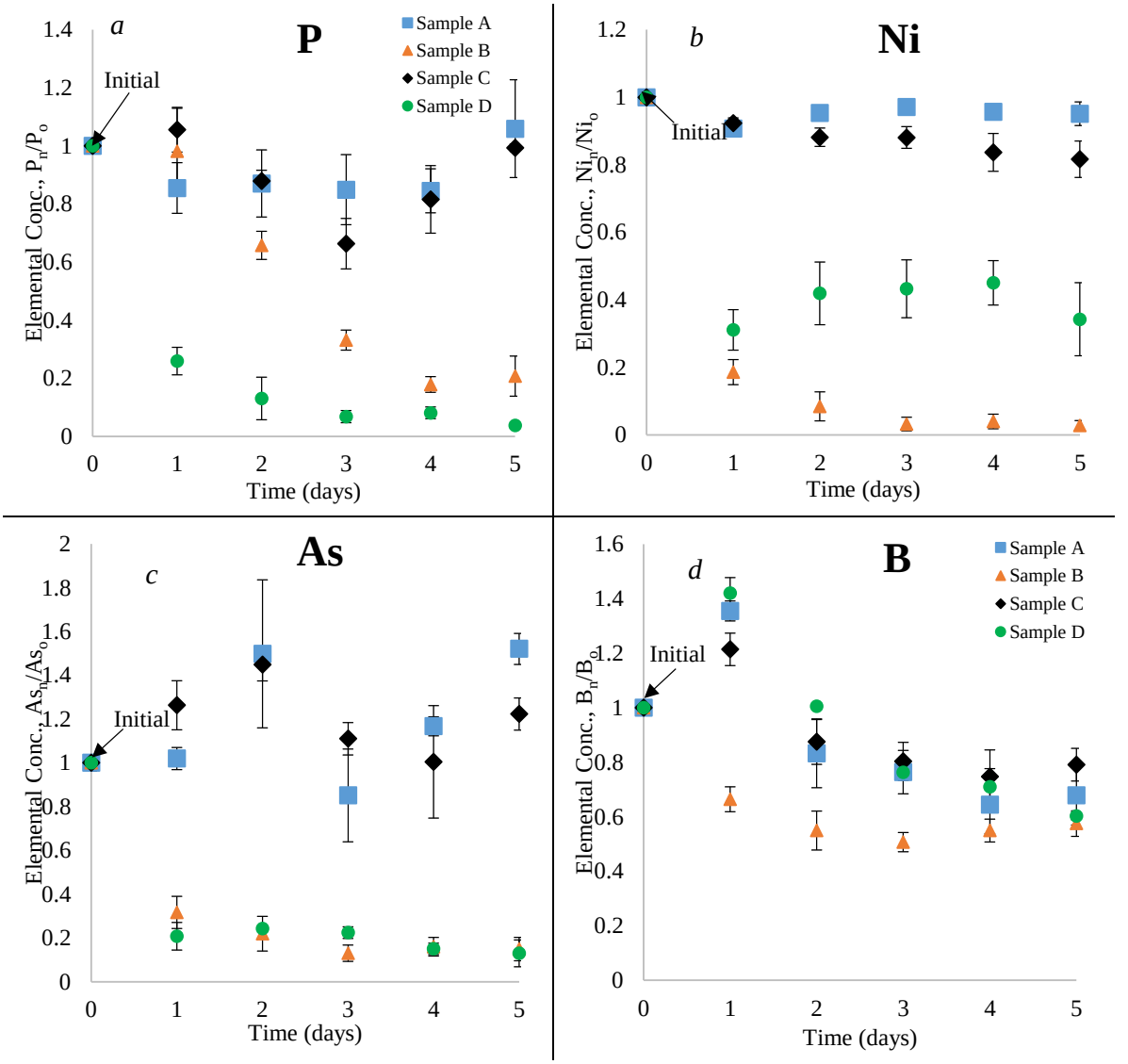

Fig. 6. Dimensionless cationic concentration of trace elements the effluent fluids showing the fraction of (a) Phosphorus (P) (b) Nickel (Ni) (c) Arsenic (As) (d) Boron (B) that were leached out from the shale rock samples. Concentrations vary significantly for this elements.

Manganese (Mn) concentration followed the trend observed in Iron (figure 4e) with sample D having a disproportionate concentration of Mn in the solution compared to the other three samples. This can be seen in figure 5a with the concentration declining exponentially during the five day experiment. The concentration of Mn in the effluent recovered for samples A, B and C were in trace amounts though sample D's fifth day concentration rapidly approached the range for these other samples. The concentration of Mn in sample D indicate a rapid reactive interaction of the manganese bearing minerals in the shale rock with CO_2 saturated brine leading to free manganese cations in solution. This Mn concentration, as with other cations, rapidly reduced over time during the experiment.

Sulphur content (figure 5b) was highest in sample D followed by samples B and A. This confirms that CO_2 saturated brine can effectively dissolve stable minerals like pyrite and other Sulphur bearing minerals. Samples B and D has the highest content of pyrite mineral as identified by XRD analysis. It appears that there is a preferential dissolution of pyrite in sample D compared to sample B, even though sample B has a higher content of pyrite. This concentration of Sulphur that was highest in sample D, had fractional values peaking within the first day of the experiment. Sample C appears lean in Sulphur content all through experiment; a stable attribute of this sample.

Figure 5c show the concentration profile for Zinc (Zn). It was also a trend of persistent concentration reduction for all the four samples analyzed. This indicates that Zn is most-likely participating in geochemical reactions as a facilitating components given its trace concentration. But given the complex reactions taking place in these heterogeneous sedimentary rocks, it is not clear where exact this free Zn attaches during reaction. The concentration of Zn in the effluent fluid associated with all the shale samples decreased compared to the initial CO_2 -brine fluid. This decrease is most pronounced in samples B and D

Interestingly, a significant concentration of Selenium were measured (figure 5d) which indicates the need to monitor ground water quality around sequestration sites. Concentrations of Selenium are most significant for samples A and C while samples B and D has little to no selenium content leached into the effluent fluid. The presence of selenium in the effluent solution showed the extent of shale rock samples' heterogeneity as no known selenium bearing mineral was identified in the rocks by XRD analysis suggesting that these selenium bearing minerals only exist in trace amount within these sedimentary rocks. The presence of free selenium in solution could act as catalysts for faster reactive flow.

The elemental concentration of Phosphorus (P) and Nickel (Ni) showed a trend of trace element consumption similar to K, Al, B and As for samples B and D. Figures 6a&b showed the trace concentrations of Ni and P. The trace profile for P indicated that samples B and D had a mild decrease in the associated effluent compared to the initial CO_2-brine fluid. Phosphorus concentration remained fairly constant for samples A and C. The trace profile for Ni indicated that samples B and D had a mild decrease in the associated effluent compared to the initial CO_2-brine fluid. Nickel concentration remained fairly constant for samples A and C. The Ni and P concentrations of A and C appeared unchanged in the effluent when compared to the influent CO_2-brine fluid These trace metals may be able to act as catalysts for surface and internal reactions in the sample rock nanopore spaces.

Arsenic and Boron elemental compositions (figures 6c and 6d) showed a similar trend to that of Aluminum for all the samples analyzed. These two elements are of concern in ensuring groundwater quality particularly in agricultural areas where carbon sequestration projects can be sited. The trace concentrations of As in the effluent fluid from samples A and C significantly diverged from samples B and D over the 5 day experiment plateauing out for all samples at end of the experiment. The minor concentrations of Boron showed a common decreasing pattern for all the samples, stabilizing towards the end of the experiment at values that are lower than the initial.

3.2 Micro-Indentation of Shale Rocks

Micro-indentation analysis were performed on polished samples of the shale rocks with the aim of determining the extent of possible changes in hardness level of the rocks after the CO_2-brine flooding experiment. The following set of conditions were used in all the indentation experiments; the maximum force used was 10 N; the loading and unloading rates were kept the same at 10 N/min; the pause at maximum load was 30 seconds; the contact load was 30 mN. The hardness was obtained with computational methods from Oliver & Pharr (2004) [22]. The indenter type was Vickers' diamond with the Poisson coefficient of 0.07. Figure 7 shows the Vickers' micro-hardness measurements acquired on the samples with error bar equivalent of standard deviation (SD) from at least three experimental runs per sample. There was noticeable decrease in the hardness of samples A, D and B in that order with sample C showing little to no change at the moderate temperature and pressure conditions in which the experiments were performed. This might indicate a weakening of the shale rocks under carbon sequestration conditions in the case of pervasive CO_2 intrusion into the overlaying caprock or most importantly at the seal rock-reservoir rock interphase where the impact of the injected CO_2 plume will be most significant. Higher temperature and pressure conditions are expected to magnify this observed impacts on shale rock geomechanics.

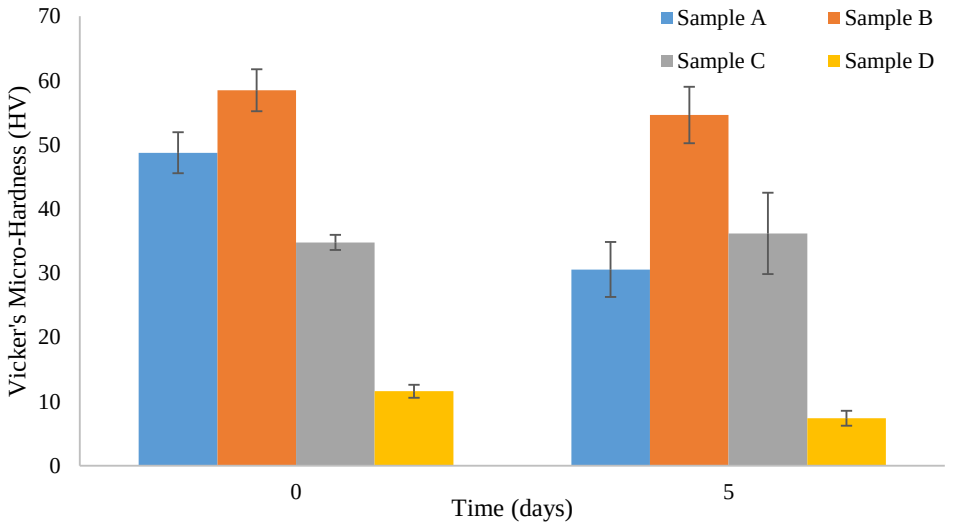

Fig. 7. The Vickers' micro-hardness measurement taken on multiple samples of the experimental shale rocks. The results indicated a mild reduction in geomechanic hardness of the rock samples which are most significant in samples A, B and D associated with lower quartz contents. This implies that initial quartz composition of shaly caprocks may be important in maintaining geomechanical integrity in long term CO_2 sequestration. Formation of diagenetic sedimentary minerals over the long term will be desired.

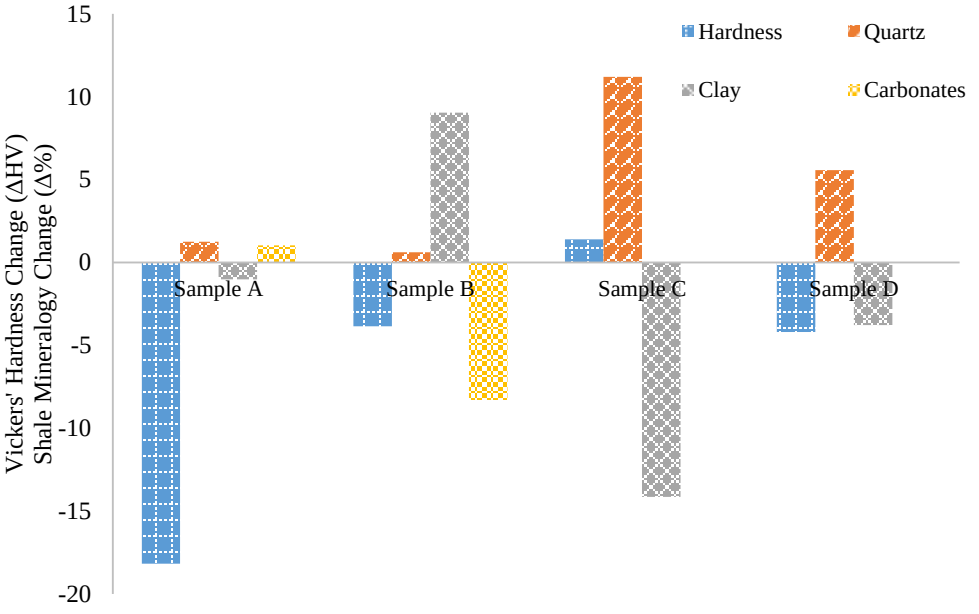

Fig. 8. A correlation between the hardness of the shale rock and quantifiable mineralogical change in percentages. The graph shows that formation of diagenetic quartz can improve the hardness of the shale rock as observed in sample C. Significant reduction in clay and carbonates fraction of the shale rock, as observed in samples A, B and D, can shrink the geomechanical hardness of the shale rock.

Figure 8 shows a correlation between the hardness of the shale rock (in absolute magnitude) and quantifiable mineralogical change in percentages as estimated from XRD analyses. The trend shows that formation of diagenetic quartz in particular can improve the micro-hardness of the shale rock as observed in sample C. Significant reduction in clay and carbonates fraction of the shale rock, as observed in samples A, B and D, could shrink the geomechanical hardness of the rock. More experimental analyses at micro- and nano-hardness levels are needed to shed more light on the long term impact of this diagenetic observations on shale rock geomechanics.

3.3 Fracture Conductivity

The fracture conductivity of the four composite cores were estimated using the modified versions of equations originally proposed by Dicman et al, and Warren and Root [23, 24] for flow in fractures; equations 1 to 8. The effective fracture width was first estimated (equation 7) and dimensionless conductivity of the cores estimated using equation 8. The major assumptions were i.) flow was primarily through micro-fractures ii.) bulk micro-fracture flow properties are captured in the experimental differential pressure measurements iii.) CO_2-brine viscosity was constant throughout the experiment iv.) the length of each of the core approximates the fracture length. The internal dimension of the multiple sets of microtubings used in the composite cores was 25um. The results of the estimated micro-fracture conductivity is similar to when experimental runs were repeated using 150μm ID size microtubings, although the gradients and theoretical exponents were noticeably different.

$$k_f = 8.45 \times 10^9 \, {w_f}^2 \qquad Eq.1$$

$$k_f = \frac{k_{av}A - k_m(A - w_f l)}{w_f l} \qquad Eq.2$$

$$8.45 \times 10^9 \, {w_f}^3 l - k_{av}A + k_m(A - w_f l) = 0 \qquad Eq.3$$

$$q_m = \frac{k_m A \Delta P}{\mu L} \qquad Eq.4$$

$$q_f = 9.86 \times 10^9 \, \frac{{w_f}^3 l \Delta P}{12 \mu L_f} \qquad Eq.5$$

$$w_f k_f = \pi C_r k L_f \qquad Eq.6$$

$$w_f = \sqrt[3]{\frac{q_f \times 12\mu}{9.86 \times 10^9 \Delta P}} \qquad Eq.7$$

$$C_r = \frac{w_f k_f}{\pi K_{av} L_f} \approx \frac{w_f}{\pi L_f} \qquad Eq.8$$

where ΔP, w_f, l, L_f, k_m, k_f, k_{av}, A, q_m, q_f, μ, and C_r represent differential pressure (atm), fracture width (cm), core diameter (cm), fracture length (cm), matrix permeability (darcy), fracture permeability (darcy), average permeability (darcy), cross sectional area (cm^2), flow rate through matrix (cm^3/sec), flow rate through fracture (cm^3/sec), viscosity (cp) and dimensionless fracture conductivity respectively. Micro-fractures are assumed to be single bundle.

Figure 9 shows the pressure responses and the dimensionless fracture conductivity for flow through the artificially fractured composite cores, calculated using equation 8. Figure 9a represents the differential pressure (dP) measured across the core and figure 9b represents the calculated dimensionless micro-fracture conductivity. The profiles

suggest that the conductivity of the micro-fractures degenerated rapidly within the first day of the experiment, tapering off at a constant rate towards the end of the experiment. This phenomenon is attributed to convective reactive transport within the artificial micro-fractures. The data presented in figure 9 were based on three experimental runs per shale rock sample with the error bar representing the standard deviation values. It is expected that larger micro-fractures will take longer experimental time to lose their conductivity as a result of short-term diagenetic alterations. A fracture conductivity loss model is being developed from this differential pressure-time dependent data set for upscaling.

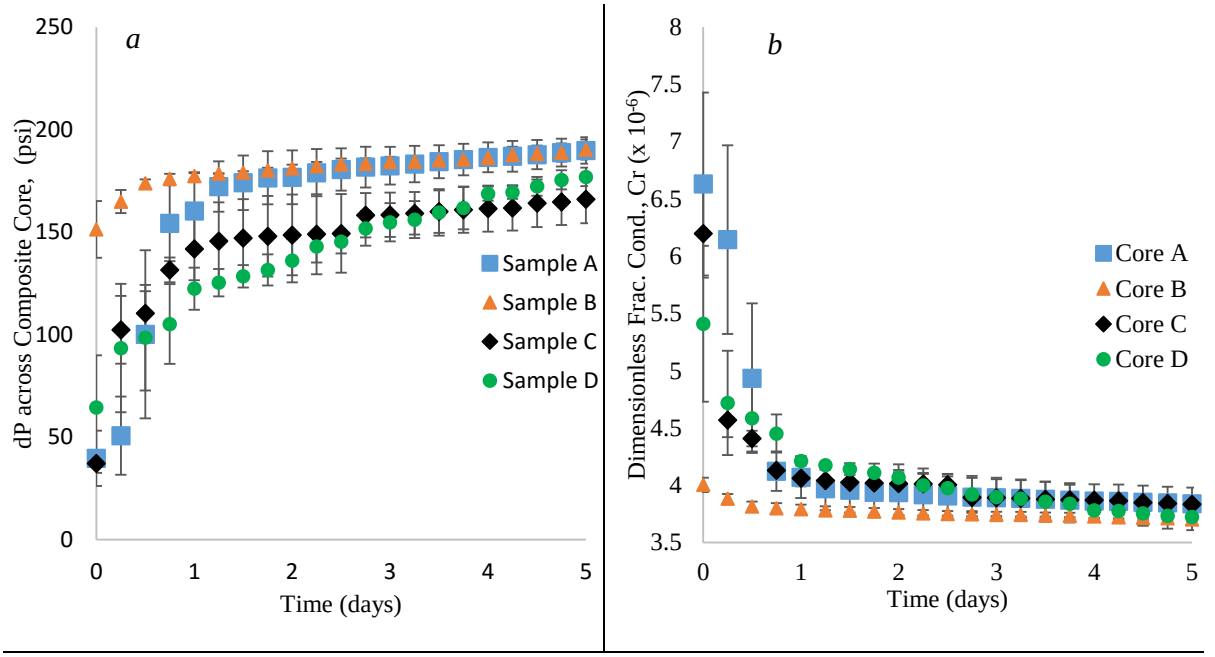

Fig. 9. (a) Average differential pressure profile across composite core, with embedded micro-tubings to mimic fractures. Each data point represented a moving average from the three experimental runs per shale rock samples.(b) Calculated dimensionless fracture conductivity profile from experimental differential pressure (dP) data using fractured core parameters. The profile indicated a rapid reduction in the conductivity of the artificial fractured core within the first two days of the experiment. This reduction can only be attributed to in-situ geochemical precipitation.

Conclusion

The geochemical interaction of shale caprock with aqueous CO_2 and its diagenetic markers have been investigated. The results presented showed that moderately high temperature and pressure in core scale experiment can lead to rapid dissolution of shale rock minerals (both clay and non-clay minerals) as shown by effluent fluid, bulk rock and precipitate analyses. Amongst the multiple elements that are leached out of the shale rocks, Calcium is predominant. This indicate that calcium based minerals in shale are the most susceptible to reactive dissolution, particularly at these experimental conditions. Furthermore, reactive dissolution led to the formation of new diagenetic minerals which precipitate out of the effluent fluid in significant quantity which can possible occlude micro-fracture defects in intact shale caprock during in-situ processes. Post flooding correlation of mineralogical composition and micro-hardness property of the bulk shale rock showed that mechanical properties of shale rocks with significant quantity of swelling clay is reduced slightly while shale rocks with increased quartz content are not affected. The differential pressure drop, its 1st derivative and estimated fracture conductivity suggests that reactive transport of dissolved minerals can possibly occlude fracture flow path, thereby improving caprock seal integrity with respect to leakage risks under CO_2 sequestration conditions.

Acknowledgements

Funding for this research work was generously provided by the Craft & Hawkins Department of Petroleum Engineering, Louisiana State University, with support from the Society of Petroleum Engineers and the GDL Foundation, Austin TX. The contributions of the members of the SEER Lab at LSU are kindly acknowledged. Thanks to Russ Lingenfelter of Engineering and Mining Experiment Station, South Dakota for generously assisting with rock comminution to preferred sizes.

References

[1] Kampman, N., Bickle, M.J, Maskell, A., Chapman, H.J, Evans, J.P., Purser, G., Zhou, Z., Schaller, M.F., Gattacceca, J.C., and Bertier, P., 2014. *Drilling and sampling a natural CO_2 reservoir: Implications for fluid flow and CO_2-fluid–rock reactions during CO_2 migration through the overburden*. Chemical Geology. 369(1): p. 51–82.

[2] Edlmann, K., Haszeldine, S. and McDermott, C. 2013. *Experimental investigation into the sealing capability of naturally fractured shale caprocks to supercritical carbon dioxide flow*. Environmental Earth Sciences. 70(7): p. 3393-3409.

[3] Noh, M.H. and Lake, L.W. 2002. *Geochemical modeling of fracture filling*. in SPE/DOE Improved Oil Recovery Symposium. Society of Petroleum Engineers. doi:10.2118/75245-MS

[4] Huerta, N.J., et al., *Reactive transport of CO_2-saturated water in a cement fracture: Application to wellbore leakage during geologic CO2 storage.* International Journal of Greenhouse Gas Control, 2016. 44: p. 276-289.

[5] Wang, J.G., et al., *A simple approach for the estimation of CO_2 penetration depth into a caprock layer.* Journal of Rock Mechanics and Geotechnical Engineering, 2016. 8(1): p. 75-86.

[6] Olabode, A. and Radonjic, M. 2013. *Experimental Investigations of Caprock Integrity in CO_2 Sequestration*. Energy Procedia 37(1): p. 5014-5025.

[7] Olabode, A. and M. Radonjic, *Characterization of Shale Cap-Rock Nano-Pores in Geologic CO_2 Containment.* Environmental & Engineering Geoscience, 2014. 20(4): p. 361-370.

[8] Olabode, A. and M. Radonjic, *Shale Caprock/Acidic Brine Interaction in Underground CO_2 Storage.* Journal of Energy Resources Technology, 2014. 136(4): p. 042901.

[9] Olabode, A. and M. Radonjic. *Characterization of Shale Rocks under Dynamic Geochemical Interaction with Brine-CO_2 Fluid*. in *47th US Rock Mechanics/Geomechanics Symposium*. 2013. American Rock Mechanics Association.

[10] Olabode, A. and M. Radonjic, *Diagenetic Influence on Fracture Conductivity in Tight Shale and CO_2 Sequestration.* Energy Procedia, 2014. 63: p. 5021-5031.

[11] Wendler, J., et al., *Carbonate diagenesis and feldspar alteration in fracture-related bleaching zones (Buntsandstein, central Germany): possible link to CO_2-influenced fluid–mineral reactions.* International Journal of Earth Sciences, 2012. 101(1): p. 159-176.

[12] Olabode, A. and Radonjic, M. 2014. *Shale Caprock/Acidic Brine Interaction in Underground CO_2 Storage.* Journal of Energy Resources Technology, 136(4): pp. 6. doi:10.1115/1.4027567

[13] Shojai Kaveh, N., A. Barnhoorn, and K.H. Wolf, *Wettability evaluation of silty shale caprocks for CO_2 storage.* International Journal of Greenhouse Gas Control, 2016. 49: p. 425-435.

[14] Selvadurai, A.P.S., *Fluid leakage through fractures in an impervious caprock embedded between two geologic aquifers.* Advances in Water Resources, 2012. 41: p. 76-83.

[15] Katsube, T.J. and Williamson, M.A. 1994. Effects of diagenesis on shale nano-pore structure and implications for sealing capacity. Clay Minerals. 29(4): p. 451-472.

[16] Kjøller, C., et al., *Novel experimental/numerical approach to evaluate the permeability of cement-caprock systems.* International Journal of Greenhouse Gas Control, 2016. 45: p. 86-93.

[17] Bobko, C.P. 2008. *Assessing the mechanical microstructure of shale by nanoindentation: The link between mineral composition and mechanical properties*. MIT. http://hdl.handle.net/1721.1/47731

[18] Bourg, I.C., *Sealing Shales versus Brittle Shales: A Sharp Threshold in the Material Properties and Energy Technology Uses of Fine-Grained Sedimentary Rocks.* Environmental Science & Technology Letters, 2015. 2(10): p. 255-259.

[19] Weaver, J.D., et al., *Fracture-Related Diagenesis May Impact Conductivity.* SPE Journal, 2007. 12(03): p. 272-281.

[20] Alemu, B.L., et al., *Caprock interaction with CO_2: A laboratory study of reactivity of shale with supercritical CO2 and brine.* Applied Geochemistry, 2011. 26(12): p. 1975-1989.

[21] Tournassat, C., et al., *Natural and Engineered Clay Barriers*. Vol. 6. 2015: Elsevier.

[22] Oliver, W.C. and G.M. Pharr, *Measurement of hardness and elastic modulus by instrumented indentation: Advances in understanding and refinements to methodology.* Journal of materials research, 2004. 19(01): p. 3-20.

[23] Dicman, A., E. Putra, and D.S. Schechter, *Modeling Fluid Flow Through Single Fractures Using Experimental, Stochastic and Simulation Approaches*. 2004, Society of Petroleum Engineers

[24] Warren, J. and P.J. Root, *The behavior of naturally fractured reservoirs.* Society of Petroleum Engineers Journal, 1963. 3(03): p. 245-255.